Overlapping microtubules establish compartments enabling the autoregulation of molecular motors

(Mol. Cell title: 3x up to 50 characters max.)

Marcus Braun*, Zdenek Lansky*, Agata Szuba, Anna Zelena,
Friedrich W. Schwarz, Aniruddha Mitra, Mengfei Gao, Annemarie Lüdecke,
Pieter Rein ten Wolde, Stefan Diez

Abstract

Collective action of molecular motors is required for the remodeling of microtubule networks underpinning essential cellular processes, such as cell division. Microtubule-crosslinking molecular motors slide microtubules along each other, yet additional regulatory proteins are thought to be necessary to control their sliding to establish stable overlaps between microtubules and prevent the breakdown of the networks. Here we show in vitro that the human kinesin-14 HSET drives microtubule sliding, which it controls by an autoregulatory mechanism. As overlapping microtubules slide apart, collectively HSET molecules detect the decreasing overlap length and slow down the sliding, leading to the formation of stable microtubule overlaps. Slowdown is quantitatively explained by the dependence of HSET sliding on the local HSET concentration in the overlap and the generation of an entropic force antagonizing the sliding. We argue that overlapping filaments, when crosslinked by proteins sensitive to their spatial arrangement, like HSET, establish envelope-free compartments with distinct microenvironments that can locally catalyze biochemical processes.

(157 of 150 words max)

Introduction

Molecular motors are enzymes that consume chemical energy to generate mechanical work. While their motor-domains step along cytoskeletal filaments, their tail-domains interact with cargo proteins, or, in some cases, interact with filaments, thus establishing crosslinks between two filaments. Concerted action of molecular motors can thus lead to sliding of overlapping cytoskeletal

filaments relative to each other, resulting in large-scale rearrangements of cytoskeletal networks. To prevent network collapse in the presence of continuous sliding by molecular motors, the regulation of molecular motor action is crucial. In particular, maintenance of stable regions of microtubule overlap requires that molecular motors are prevented from sliding microtubules apart fully. One example of such motor regulation, is in the midzone of the mitotic spindles during cell division. There, microtubules emanating from the opposite spindle poles are crosslinked by molecular motors, which slide the microtubules along each other. Importantly, however, these overlaps are stable over tens of minutes (Schuyler et al., 2003; Yamashita, 2005).

For this regulation, additional proteins are thought to be necessary. Examples are kinases and other protein-modifying enzymes, which conduct direct posttranslational modifications of the molecular motors (e.g. phosphorylate them), or influence the motors indirectly by modifying other regulatory proteins (Andrews et al., 2004; Cahu et al., 2008; Fu et al., 2009; Khmelinskii et al., 2009; Mana-Capelli et al., 2012). Moreover, motor action can be regulated by other motors that generate force in the opposite direction. This regulation, however, does not lead to the formation of stable regions of microtubule overlap, but instead leads to directional instability of microtubule sliding, manifested by the sequential switching of sliding from one direction to the other (Hentrich and Surrey, 2010; Tao et al., 2006). Finally, molecular motors can be regulated by diffusible non-motor microtubule crosslinkers, which can act as brakes for motor-driven sliding. In contrast to the regulation by opposing motors, the presence of crosslinkers can lead to the progressive slowdown of motor-driven sliding and to the formation of stable microtubule overlaps (Braun et al., 2011; Johann et al., 2015).

We here report on a different way of regulating the collective action of molecular motors, distinct from the aforementioned mechanisms. We show that, without the need for additional regulatory proteins, autoregulation of molecular motors can result from the interplay between the spatial arrangement of microtubules and the structure of the molecular motors themselves. In particular, we found that kinesin-14 HSET molecular motors (a) slide microtubules relative to each other, and (b) are sensitive to the changes in the

length of the microtubule overlap region, and, through an autoregulatory mechanism, slow down sliding when the microtubules start separating. HSET molecules by themselves thus establish stable overlaps between microtubules. We quantitatively explain the autoregulation by the preferential binding of HSET to regions of microtubule overlaps, which thus constitute compartments with distinct microenvironments. When the two microtubules start sliding apart, the preference results in the increase in local concentration of HSET in regions of microtubule overlap, leading to HSET density-dependent reduction of sliding velocity through steric hindrance between the motors and an opposing entropic force generated by the overlap-bound motors. We argue that autoregulation in response to microenvironments, established by cytoskeletal filament-based compartmentalization, is a ubiquitous mechanism that applies not only to specialized molecular motors like HSET but, analogously, is applicable to a range of other proteins.

Results

HSET-propelled microtubule sliding slows down when microtubules start to slide apart

To study the microtubule crosslinking activity of HSET we immobilized dimly rhodamine-labeled 'template' microtubules on a coverslip and allowed GFP-HSET to interact with the microtubule lattice. When we added brightly rhodamine-labeled 'transport' microtubules, we observed the formation of microtubule overlaps and, in presence of ATP, we observed directed microtubule sliding at constant velocity (Figure 1, Methods). Consistent with previous results on *D. melanogaster* kinesin-14 Ncd (Fink et al., 2009), we found that GFP-HSET crosslinks microtubules into both parallel and antiparallel geometries, but slides only antiparallel ones (Figure S1). Importantly, in contrast to GFP-Ncd (Braun et al., 2011), we found that GFP-HSET preferentially interacts with overlapping microtubules (as opposed to non-overlapping single microtubules), following the region of microtubule overlaps during microtubule sliding (Figure 1B,C). We estimated the density of GFP-HSET in the overlap as the integrated GFP intensity along the length of the overlap, divided by the overlap length (for details see Methods). We found that, at 1.5 nM GFP-HSET in solution, the density of GFP-

HSET in overlaps was approximately six times higher than on single microtubules, demonstrating that the affinity of GFP-HSET for the overlap region is significantly higher than the GFP-HSET affinity for single microtubules

Previous work on kinesin motors showed that transport microtubules continue to slide along template microtubules with constant velocity until their ends fully separate (Braun et al., 2009; Fink et al., 2009; Hentrich and Surrey, 2010; Kapitein et al., 2005; Sturgill et al., 2014). By contrast, we found that HSET-driven transport microtubules that initially moved steadily towards the minus-ends of template microtubules, slowed down markedly when the microtubules started to slide apart (Figure 1B,C and Supplementary Movie S1). This slowdown in sliding resulted in the formation of microtubule overlaps, which were stable for about 20 minutes. This observation suggests that, unlike other kinesin motors, human kinesin-14 regulates the velocity of microtubule-microtubule sliding in a manner that depends on the length of the microtubule overlap.

HSET driven microtubule sliding slows down with increasing density of motors in the overlap

To investigate the adaptive sliding by HSET we quantitatively analyzed the sliding velocities and the amount of GFP-HSET molecules in the shortening overlaps during events such as those presented in Figure 1. We found that the total intensity of GFP-HSET molecules in the shortening overlaps remained constant as the microtubules slid apart, meaning that the density of GFP-HSET in the overlap regions progressively increased (Figure 2A, S2A). This finding suggests that the ends of the microtubule overlap region constitute barriers that GFP-HSET molecules are not able to cross. The two barriers, which converge as the microtubules slide apart, thus herd the GFP-HSET molecules in the overlap region. Time-lapse video analysis revealed that the velocity of microtubules sliding apart decreased with the increasing density of HSET in the microtubule overlap (n = 33 microtubules; Figure 2B).

As the amount of GFP-HSET in the overlap stayed constant during the observed slowdown in sliding velocity, we reasoned that the slowdown is due to the increased density of GFP-HSET molecules in the shortening overlap. We thus asked whether an increase in GFP-HSET density can also slow down the sliding

velocity of microtubules that are not sliding apart, but are overlapping fully. We analyzed the sliding velocities of those transport microtubules that were in contact with the template microtubules over their full lengths. Similarly to the results presented for separating microtubules, we found that the sliding velocity of fully overlapping microtubules decreased with increasing density of GFP-HSET molecules in the overlap (n = 67 microtubules; Figure 2C). Intriguingly, we observed that for a given GFP-HSET density the separating microtubules were sliding on average slower than microtubules overlapping fully (repeated measures ANOVA, $p < 10^{-4}$; compare Figs. 2B and 2C). This finding suggests that not only the increase in density, but also the geometry of the microtubule assembly plays a role in the slowdown of sliding and the generation of stable overlaps observed in Figure 1.

Due to the high level of noise in the data presented in Figures 2B and 2C, we aimed to assess the influence of the motor density on the microtubule sliding velocity in an independent way. We thus performed a set of complementary experiments in which we coated the coverslip using decreasing concentrations of GFP-HSET molecules in solution, resulting in decreasing densities of GFP-HSET molecules bound to the coverslip surface, thus tuning the spacing between the GFP-HSET molecules. We then let microtubules glide along such a glass surface coated with GFP-HSET and determined the microtubule gliding velocities (Methods). We found that a reduction in the concentration of GFP-HSET resulted in an increase in microtubule gliding velocities (Figure 2D). This increase in velocity is likely not due to the change in the absolute numbers of molecular motors, because we observed, at any of the given molecular motor densities, that longer microtubules (with more molecular motors attached) glided with the same velocity as shorter microtubules (with less molecular motors attached; Figure S2B). This result shows that the density of GFP-HSET motors (i.e. the spacing between the molecular motors) determines the velocity of the microtubule movement.

To exclude any possible influence of the N-terminal tail-domain of HSET, which in other kinesin-14 family members is known to interact with microtubules (Braun et al., 2009; Fink et al., 2009; Hentrich and Surrey, 2010) and could thus hinder the microtubule movement, we created a truncated GFP-

HSET construct, lacking the tail-domain (for details on this construct please refer to Figures 3C and S3C). We repeated our microtubule gliding experiments using this truncated HSET construct and obtained qualitatively identical results, i.e. the gliding velocity did not depend on the length of the gliding microtubules, but did depend on the surface density of HSET on the coverslip surface (Figure S2C). Taken together these experiments demonstrate that at increased density HSET molecular motors propel microtubule translocation at decreased velocities.

HSET diffusion constant is decreased in microtubule overlaps as compared to single microtubules

To assess the molecular mechanism of HSET confinement to regions of microtubule overlap (which is a prerequisite for the HSET density increase in shortening overlaps) we next characterized the interaction of individual GFP-HSET molecules with both single and overlapping microtubules in presence of ATP. We formed microtubule overlaps similarly to the experiment presented in Figure 1 using low concentration (0.15 nM) of non-labeled HSET. After addition of GFP-HSET we observed diffusible interaction of GFP-HSET with single microtubules and with microtubules in the overlap region. Analyzing the free diffusion regime of single GFP-HSET molecules, we obtained the diffusion constants of 0.39 ± 0.01 $\mu m^2 s^{-1}$ (± SEM) for the diffusion of GFP-HSET on single microtubules and 0.021 ± 0.005 $\mu m^2 s^{-1}$ (± SEM) for the diffusion of GFP-HSET in regions of microtubule overlap (Figure 3A and S3A, S3B). We attribute this drastic reduction of the diffusion constant, by more than an order of magnitude, to the simultaneous interaction of GFP-HSET molecules with both microtubules in regions of overlap. To address the question if the ATPase activity of the motor is required to reduce the HSET diffusion constant in regions of microtubule overlap we used full-length HSET and exchanged the ATP-containing buffer for a buffer containing ADP. Under these conditions, the observed diffusion looked similar to the diffusion in the presence of ATP, both on single microtubules and in the microtubule overlaps (Figure 3B), indicating that the nucleotide state of the motor-domain has no influence on the HSET diffusibility. In both cases, in the presence of ATP or ADP, we frequently observed individual GFP-HSET molecules switching from fast to slow diffusion when the molecules moved from single

microtubule to microtubule overlap (Figure 3A, event marked by red arrow). On rare occasions we observed a single GFP-HSET molecule moving out of the overlap region and switching from slow to fast diffusion (Figure 3A, event marked by black arrow) indicating that the transition from a region of overlap onto a single microtubule is possible, but energetically unfavorable. In combination, these experiments demonstrate on a single molecule level the presence of diffusion barriers at the ends of microtubule overlaps as observed in Figure 1. These barriers, at either side of the region of overlap, effectively confine the movement of GFP-HSET to the region of microtubule overlap once a molecule is trapped in this region. Importantly, diffusibility of the GFP-HSET molecules in the microtubule overlap allows the GFP-HSET molecules to follow the region of overlap when the microtubules are sliding and the diffusion barriers move.

The two microtubule-binding sites of HSET have distinct binding characteristics

The specific interactions of GFP-HSET with microtubules depend on the two microtubule-interaction sites at the opposing end of the HSET primary sequence, termed the motor- and tail-domain, respectively. We therefore next aimed to dissect the relative contributions of these two interaction domains on the GFP-HSET diffusion, both inside and outside of regions of microtubule overlap. Based on computational predictions of the position of the kinesin motor-domain and coiled-coil dimerization regions in HSET molecules in addition to structural information available from other kinesin-14 family members (Chandra et al., 1993; Karabay and Walker, 1999; Lupas et al., 1991), we generated two truncated homodimeric GFP-HSET constructs consisting of the coiled-coil with either only the HSET motor-domain (GFP-HSET-motor) or only the HSET tail-domain (GFP-HSET-tail) (Figure 3C, Figure S3C, Methods). Using the truncated constructs we first attempted to form microtubule overlaps. We varied the concentrations of GFP-HSET-tail and GFP-HSET-motor-domain up to 75 nM each, but we never observed the formation of microtubule overlaps, demonstrating that motor- and tail-domain microtubule binding sites are required simultaneously to form a crosslink between two microtubules.

To describe the individual contribution of the HSET motor- and tail-domains to HSET diffusibility, we allowed the interaction of our truncated constructs with both single microtubules and microtubule overlaps (pre-formed by previous incubation with 0.15 nM unlabeled full-length HSET). We found that on single microtubules the interaction time of the GFP-HSET-tail is on the order of minutes, with a diffusion constant of 0.41 ± 0.02 $\mu m^2 s^{-1}$ (± SEM) (Figure 3D, Figure S3D). This diffusion constant of the GFP-HSET-tail on a single microtubule was not significantly different from the diffusion constant of the full length GFP-HSET on a single microtubule, suggesting that the full length HSET interacts with a single microtubule predominantly via its tail-domain, which is consistent with previous work on *D. melanogaster* kinesin-14 (Fink et al., 2009). Interestingly, in contrast to the full-length GFP-HSET construct, we observed that the GFP-HSET-tail diffuses within the microtubule overlaps in the same way as on single microtubules and that it diffuses freely across the overlap ends (Figure 3D; events marked by arrows).

Using the GFP-HSET-motor construct, we then set out to determine how the motor-domain of HSET (in ATP) interacts with microtubules. We observed very short interactions of GFP-HSET-motor molecules both with individual microtubules and with regions of microtubule overlap, with a rate of unbinding of 4.1 ± 0.9 s^{-1} (95 % confidence interval) from both (Figures 3E, S3E). Thus, similarly to GFP-HSET-tail, GFP-HSET-motor does not distinguish between single microtubules and regions of microtubule overlap. Since the interaction time of the GFP-HSET-motor is very short, we were unable to reliably detect any movement of the molecules along the microtubule. In combination, these experiments show that both interaction sites are required for the HSET molecule to recognize the position of the overlap. The tail-domain maintains a constant rate of diffusion independent of whether it moves on single microtubules or inside the overlap. Importantly, this rate is equal to the diffusion rate of the full length HSET on single microtubules. It is thus the interaction of the motor-domain of full-length HSET with an adjacent microtubule that lowers the rate of HSET diffusion in the overlap.

HSET motors confined in partial overlaps generate entropic force, which helps stabilizing the microtubule overlap region

We have seen that increased density of HSET in microtubule overlaps decreases the velocity of microtubule sliding. However, for given GFP-HSET densities the separating microtubules were sliding slower than fully overlapping microtubules (Figs. 2B and 2C), showing that the density-dependence of HSET-driven sliding can not fully explain the formation of stable overlaps observed in Figure 1. Our single molecule experiments revealed that HSET diffuses in the microtubule overlap and that its diffusion, in presence of either ATP or ADP, is confined to the region of overlap. In our previous work we demonstrated that diffusible microtubule crosslinkers confined in an overlap between two microtubules generate entropic forces that promote an increase in overlap length (Lansky et al., 2015). We thus asked whether, analogously, HSET molecules confined in a partial microtubule overlap generate entropic forces that would counteract their motor-domain-generated force that drives the microtubules apart. To address this question, we aimed to decouple the ATP-dependent motor-domain-generated force from the putative ATP-independent entropic force. To do this, we formed the overlaps similarly as in the experiment presented in Figure 1, but using a motility buffer containing ADP instead of ATP. In this scenario GFP-HSET was able to crosslink microtubules, but did not induce their relative directional sliding because its motor-domain activity was disabled (0 % sliding events from the total of n = 36 observed fully overlapping microtubule pairs). To move the transport microtubules relative to the templates, we then used hydrodynamic flow of the motility buffer, which also removed unbound HSET from solution. Partial overlaps were created when the transport microtubules started sliding over the ends of their templates due to the buffer flow, thus decreasing the lengths of the overlaps between the microtubules. After stopping the hydrodynamic flow, we observed that the transport microtubules started moving in the direction of increasing overlap lengths (Figure 4). We observed neither movement of partially overlapping microtubules in the direction decreasing the overlap length nor did we observe any directional movement of transport microtubules that fully overlapped with their templates. This finding demonstrates that GFP-HSET molecules confined

between partially overlapping microtubules can generate a force, which moves microtubules in the direction that increases the length of the microtubule overlap, independent of ATP hydrolysis. We estimated the amount of HSET molecules in the overlap during this overlap expansion and found that it is constant (Figure S4), showing that the overlap expansion is not driven by a change in enthalpy induced by binding of HSET molecules from solution into the overlap region. Analyzing the sliding velocities we found that they were inversely proportional to the length of the overlap (Figure 4D). These findings suggest that molecules of HSET generate entropic forces, similar to microtubule crosslinkers of the PRC1/Ase1/MAP65 family (Lansky et al., 2015) .

To measure the magnitude of this entropic force we used optical tweezers combined with confocal microscopy. We created partial microtubule overlaps by specifically attaching two microtubules to two polystyrene beads and bringing the two beads in close proximity by two optical traps in presence of GFP-HSET and ADP in solution (Methods). After the overlap was established, we pulled the two microtubules apart by steadily moving one of the traps relative to the other (Figure 4E). As the overlap between the two microtubules decreased, we observed an increasing force opposing the trap movement (Figure 4F and 4G). The force reached values up to ~ 4pN just before the microtubules were pulled apart (Figure 4G).

Taken together these results show that HSET confined in an overlap generates an entropic force, analogous to confined gas particles generating a pressure. Consequently, when HSET slides microtubules apart, such as in the experiment in Figure 1, the motors have to work against this increasing entropic force as the length of the overlap between the microtubule decreases.

Low diffusion constant of GFP-HSET in regions of microtubule overlap is explained by a high rate of motor-domain binding to the microtubule due to high local concentration

We next asked whether we can quantitatively explain the slowdown of HSET driven sliding in microtubule pairs that slide apart starting from the basic principles of the interaction between HSET and microtubules, using the experimental knowledge of the two microtubule-interaction sites of HSET. We

thus performed a set of numerical simulations of HSET molecules interacting with two microtubules. We simulated the HSET molecules as harmonic springs, whose one end (the tail-domain interaction site) can hop randomly along a one-dimensional array of binding sites on one filament and whose other end (the motor-domain interaction site) hops directionally along a one-dimensional array of binding sites on the second filament (Figure 5A; Methods). The hopping rates and the rates of unbinding of the two interaction sites from the filaments were determined from the experimentally measured values. Since, on a single microtubule, the tail-domain has a much longer interaction time than the motor-domain, at any given time, most HSET molecules are anchored to a microtubule via their tail-domains, with motor-domains facing outwards. An anchored HSET molecule, scanning the surface of the microtubule by tail-mediated diffusion, can - when located in a region of microtubule overlap - bind to the adjacent microtubule via its motor-domain. The time for the motor-domain of this anchored HSET molecule to find via diffusion a microtubule binding-site is much shorter than that for the motor-domain of an HSET molecule freely diffusing in the bulk solution. Anchoring raises the effective local concentration of the head-domains, making the local concentration inside the overlap, $c_{\text{anchor,}}$ larger than that in solution, c_{solution}. Since the net binding rate at which a motor-domain will bind is given by the association rate constant k_{on} times the local concentration c, the net binding rate for an anchored domain inside the overlap, $k_{\text{on}}^{\text{motor(anchor)}} = k_{\text{on}}\, c_{\text{anchor}}$ is larger than that for an unanchored domain in solution, $k_{\text{on}}^{\text{motor(solution)}} = k_{\text{on}}\, c_{\text{solution}}$. The overlap region can thus be described as a specific microenvironment characterized by an increase in the local concentration of HSET, which raises the binding rate (Figure 6A).

First, we aimed to explain the motion of a single HSET molecule in the microtubule overlap. To capture the motion of a single HSET molecule between two filaments we varied in the simulations the unknown net binding rate $k_{\text{on}}^{\text{motor(anchor)}}$ and observed that the rate of diffusion of the molecules decreased as $k_{\text{on}}^{\text{motor(anchor)}}$ was increased. Increasing the rate of anchored motor-domain binding means that an HSET molecule is more often bound to both microtubules inside the overlap, which drastically slows down its diffusion. We found that the experimentally observed value of the diffusion constant was reproduced for the

binding rate $k_{on}^{motor(anchor)}$ of 60 s^{-1} (Fig 5B). This result means that after the experimentally determined dwell time of the motor-domain bound to the microtubule of about 0.3 s, the motor-domain will rebind rapidly within $1/k_{on}^{motor(anchor)}$ = 0.017 s. In this time the HSET molecule can move by its tail-mediated diffusion only a very short distance, meaning that HSET molecules, at the ends of the microtubule overlap regions, are very likely to re-bind by their motor-domains to the overlap region and are therefore unlikely to leave the overlap. Our simulations thus explain both i) the experimentally observed slower diffusion of HSET inside the overlap and ii) the confinement of the HSET molecules to regions of microtubule overlap, which is due to the interplay between the spatial arrangement of the microtubules and the HSET binding kinetics.

Confinement of diffusible HSET molecules in the microtubule overlap explains the slowdown of microtubule sliding when microtubules start to separate

We have experimentally shown that an increase in the density of HSET in the overlap between microtubules that are sliding apart slows down the sliding (Figure 2). We hypothesize that this slowdown can be explained by the confinement of HSET to the region of microtubule overlap. To test this hypothesis we performed simulations, keeping all the parameters as determined above for single HSET molecules. We first simulated the sliding of a transport microtubule that fully overlaps with a template microtubule. We varied the density of HSET molecules in the microtubule overlap (by changing the length of the transport MT while keeping the total number of HSET molecules inside the overlap constant) and, similarly to our experiments, we observed that the sliding velocity decreases with increasing motor density (Figure 5C).

Next we simulated the experiments in which two microtubules are connected by HSET molecules, forming a partial overlap in the presence of ADP (and in the absence of ATP). We simulated this nucleotide condition by setting the maximum force that the motor can generate to zero. As observed in the experiments we see that the filaments move in the direction of increasing overlap length and that the velocity of sliding is inversely proportional to the

length of the overlap (Fig 5D,E). This effect is due to the entropic expansion force that is generated by the diffusible HSET molecules confined inside the overlap region.

Finally, we simulated the situation in which a transport microtubule slides off a template microtubule (Figure 5F-H). Similarly to the experiment presented in Figure 1, we observe that as the microtubules start to separate and the region of microtubule overlap shortens, HSET molecules get compacted in that region leading to an increase in HSET density (Figure 5F,G and S5A). With increasing HSET density the velocity of sliding decreases (Figure 5H) resulting in the formation of a stable microtubule overlap (Figure 5F). Our simulations are consistent with the observation (Figures 2B and 2C) that for a given HSET concentration the sliding velocity is on average higher for transport microtubules that overlap with the template microtubules over their full length as compared to transport microtubules that slide apart and thus overlap with the template microtubules only partly (repeated measures ANOVA, $p < 10^{-4}$; compare Figures 5C and 5H). This difference is due to the entropic force, which can manifest itself only when the size of the overlap region can change, which is the case only when the microtubules overlap partly. Our simulations thus enable us to differentiate between the two effects that lead to the decrease in sliding velocity during the microtubule separation, namely the i) the HSET-density dependence of the sliding velocity and ii) the entropic force acting against the motor-domain generated force. Our simulations thus show that the confinement of HSET to the overlap region of separating microtubules increases the HSET density in the overlap, which slows down, and ultimately halts, the separation of the microtubules.

Together, our experimental and theoretical results reveal a novel feedback mechanism, which prevents the HSET-driven microtubules from full separation (Figure 6B). When the overlapping microtubules start to slide apart, the converging overlap ends herd the HSET molecules, increasing their density in the overlap. The rise in density reduces the microtubule sliding velocity and increases the resisting entropic force, resulting in the formation of stable overlaps between the microtubules.

Discussion

HSET combines in itself the features of a molecular motor and a diffusible crosslinker

The collective action of molecular motors leading to relative sliding of microtubules is essential for the remodeling of microtubule networks during the cell cycle. HSET is known to slide short, nascent microtubules towards the spindle poles (Cai et al., 2009) and, in concert with other microtubule sliding motors like kinesin-5 and dynein, HSET is involved in the focusing of the spindle poles (Goshima et al., 2005; Kwon et al., 2008; Lecland and Lüders, 2014; Watts et al., 2013). *In vitro* investigation of microtubule sliding revealed that all molecular motors known to slide microtubules, such as kinesin-5 Eg5, the kinesin-12 Kif15 as well as the kinesin-14 family members Klp2, XCTK2 and Ncd, slide the microtubules apart completely (Braun et al., 2009; Fink et al., 2009; Hentrich and Surrey, 2010; Kapitein et al., 2005; Sturgill et al., 2014). Molecular motors, therefore, have to be regulated to prevent the complete separation of sliding microtubules, necessary to maintain the integrity of the cytoskeletal networks. *In vivo* experiments show that diffusible crosslinkers of the PRC1/Ase1/Map65 family are essential for the establishment and maintenance of stable bipolar structures, like the *S. pombe* interphase microtubule array (Janson et al., 2007) or the midzone of mitotic spindles (Schuyler et al., 2003; Yamashita, 2005). *In vitro,* it has been confirmed that the diffusible crosslinker Ase1, which preferentially binds to microtubule overlaps, regulates the motor-driven microtubule sliding: When microtubules start to slide apart Ase1 prevents the microtubule separation and enables the formation of stable microtubule overlaps via two coexistent mechanisms: i) relative increase in the ratio of crosslinkers and motors in the shortening overlap, manifested by a relative increase in friction, leading to the slowdown of sliding (Braun et al., 2011) and ii) confinement of diffusible Ase1 molecules in the shortening overlap, leading to the generation of an entropic expansion force that opposes the motor-propelled sliding (Lansky et al., 2015). We here show that the human kinesin-14 HSET combines in itself the features of a molecular motor that slides microtubules and a diffusible crosslinker that slows down the sliding when the two microtubules start to slide apart. Like Ase1, HSET has a preference for

binding to the overlap, and is thus retained in the overlap when two microtubules are sliding apart. This leads to an increase in HSET density, which, we argue, causes the reduction in sliding velocity. HSET can thus effectively act as its own brake, leading to the autoregulation of HSET-induced overlap formation.

HSET is sensitive to changes in overlap length and adapts the sliding velocity through an autoregulatory mechanism

Of all molecular motors that are known to slide microtubules, HSET is the only one that decelerates when the microtubules start separating. Other motors fail to slow down, because, unlike HSET, they are not sensitive to regions of microtubule overlap and do not preferentially bind to those regions, which is well documented in the case of Ncd (Braun et al., 2011). Thus, the other molecular motors maneuver a radically different energy landscape than HSET, a landscape in which the ends of microtubule overlaps, rather than being impassable barriers, are undetectable. By contrast, HSET, confined by diffusion barriers at the ends of regions of microtubule overlap, is locally concentrated in the overlap. Concentration of HSET molecules, manifested by high HSET density in the overlap, regulates the sliding in two ways. (1) The sliding velocity decreases with increasing HSET density. This effect can be explained by either a decrease in the collective motor force driving the sliding or an increase in friction between the overlapping microtubules. We hypothesize that these effects might be due to steric hindrance between the motors. In our simulations we observe individual molecules in the overlap frequently coming into contact with each other. Experimentally, likewise, mean square displacement analysis of the motion of single GFP-HSET molecules in the overlap suggests that HSET molecules cannot pass each other in the microtubule overlap and thus hinder each others motion (Figure S3B). (2) HSET is regulated through an entropic force generated by the HSET molecules confined in the overlap. HSET entropic force generation provides a new example of a general mechanism of entropic expansion of confined diffusible crosslinkers described earlier (Lansky et al., 2015). Diffusibility of the crosslinker in the overlap is a prerequisite for this mechanism. Although HSET does not have two diffusible microtubule-binding

sites, nevertheless, due to its motor-domain with a very high rate of binding and unbinding from the microtubule, HSET molecules effectively act as diffusible crosslinkers in the overlap.

An additional force, antagonizing HSET motor driven sliding, leading to an extra layer of regulation of the motor-driven sliding force, might be generated by the changes in enthalpy when HSET molecules bind from solution to the microtubule overlap (Lansky et al., 2015). Combined, these effects lead to an autoregulatory mechanism that detects the changes in the length of the microtubule overlap and, accordingly, changes the velocity of HSET-driven microtubule sliding.

The ends of the microtubule overlap act as a switch for the rate of HSET binding to the microtubules

The autoregulatory mechanism of the collective action of HSET is based on the fact that HSET molecules are sensitive to the presence of microtubule overlaps. HSET binds to microtubules predominantly with its tail and scans the surface of the microtubule via diffusion along the microtubule lattice. When it encounters a second, adjacent, microtubule during this process, it swiftly interacts with it via its motor-domain. At a given concentration of HSET in solution, the rate at which an HSET motor-domain anchored to one microtubule binds to the adjacent microtubule in the overlap region will be much higher than that at which an unanchored HSET motor-domain binds a single microtubule from solution. This is because in the overlap region the motor-domains are held close to their binding sites by the interaction of the tail-domains with the anchoring microtubule. The overlap boundary thus acts as a switch for the binding rate of the motor-domain. When an HSET molecule diffusing within the overlap region encounters the end of an overlap it has a low probability of leaving the overlap. We explain this low probability by the fact that when the motor-domain unbinds, the HSET molecule can diffuse only a short distance along the surface of the microtubule by its tail-domain before the motor-domain rebinds. Given the length and flexibility of the HSET molecule, it is very likely to rebind back to the overlap. Individual GFP-HSET molecules can thus easily cross this boundary towards a region of the overlap but are unlikely to cross the

boundary in the opposite direction, towards the single microtubule. The boundaries at the end of the overlap region thus compartmentalize bundled microtubules, creating microenvironments with distinct HSET-microtubule interaction kinetics.

The arrangement of microtubules into bundles creates envelope-free compartments

HSET autoregulation is based on the local microenvironment of the microtubule overlap, which yields a high local concentration of HSET motor domains. The consequences of the higher local concentration are on two levels: i) it creates a high affinity of the HSET molecules for the overlap as described in the previous paragraph and ii) this high affinity for the overlap, in turn, leads to an increase in HSET density, which results in the autoregulation and the slowdown of sliding. The high local concentration of HSET motor-domains enables HSET to maintain the crosslink between two microtubules despite being a non-processive motor with high unbinding rates of its motor-domain from isolated microtubules. Some dimeric molecular motors, such as kinesin-1, maintain processivity by a mechanism based on a similar effect. The microtubule-bound motor-domain of kinesin-1 positions the other motor-domain in a close proximity to its binding site, creating thus a microenvironment with strongly increased on-rate of the tethered motor-domain hovering over its binding site.

The establishment of compartments with local microenvironments is a general cellular strategy (Hyman et al., 2014; Patel et al., 2015), enabling reactions that would not happen in the homogenous cytoplasm due to the insufficiently low concentrations of the reactants. The prime example of this principle is organelles, which are separated from the rest of the cytoplasm by a lipid envelope. However, many different envelope-free structures, like lipid rafts or liquid-liquid phase separated nucleoli or stress granules in the cytoplasm, may act as concentrators, which constitute microenvironments that effectively trap molecules. Here we show that microtubule overlaps establish local microenvironments, which enable HSET to detect and act against a decrease in the overlap length. We thus argue that spatial arrangements of cytoskeletal

filaments, such as regions of microtubule overlap, can act as envelope-free compartments, which establish microenvironments that locally promote specific biochemical reactions.

Acknowledgements

We thank the members of the Diez laboratory for fruitful discussions, Claire Walczak (Indiana University, Bloomington, IN, USA) for HSET plasmid DNA used as PCR template and Gero Fink (formerly MPI-CBG, now MRC Cambridge UK) for first experiments on HSET-propelled microtubule sliding and participation in the purification of the first batch of recombinant GFP-HSET proteins. Financial support from the European Research Council (ERC starting grant 242933 to SD), the Deutsche Forschungsgemeinschaft (Heisenberg programme grant DI 1226/4 and research unit SFG 877 grant DI 1226/5), Center for Advancing Electronics Dresden (cfaed), ESF (contract 100111059, MindNano), the Dresden International Graduate School for Biomedicine and Bioengineering (stipend to AL), the Czech Science Foundation (grant no. 15-17488S to ZL), the project "Introduction of new research methods to BIOCEV" (CZ.1.05/2.1.00/19.0390) from the ERDF and institutional support of the Institute of Biotechnology RVO: 86652036 is acknowledged. We furthermore thank the Technische Universität Dresden and the Max Planck Society. This work is part of the research programme of the Foundation for Fundamental Research on Matter (FOM), which is part of the Netherlands Organisation for Scientific Research (NWO).

Author contributions

Experiments were conceived by MB, ZL and SD, performed by MB, ZL, AZ, AS, AM, MG and AL, and analyzed by MB, ZL, AZ, AS, AM, MG, AL and FWS. MB, ZL, PRtW and SD developed the mathematical model and wrote the manuscript. All authors discussed the results and commented on the manuscript.

References

Alper, J.D., Tovar, M., and Howard, J. (2013). Displacement-Weighted Velocity Analysis of Gliding Assays Reveals that Chlamydomonas Axonemal Dynein Preferentially Moves Conspecific Microtubules. Biophys J *104*, 1989–1998.

Andrews, P.D., Ovechkina, Y., Morrice, N., Wagenbach, M., Duncan, K., Wordeman, L., and Swedlow, J.R. (2004). Aurora B regulates MCAK at the mitotic centromere. Dev Cell *6*, 253–268.

Braun, M., Drummond, D.R., Cross, R.A., and McAinsh, A.D. (2009). The kinesin-14 Klp2 organizes microtubules into parallel bundles by an ATP-dependent sorting mechanism. Nat Cell Biol *11*, 724–730.

Braun, M., Lansky, Z., Bajer, S., Fink, G., Kasprzak, A.A., and Diez, S. (2013). The human kinesin-14 HSET tracks the tips of growing microtubules in vitro. Cytoskeleton (Hoboken, NJ) *70*, 515–521.

Braun, M., Lansky, Z., Fink, G., Ruhnow, F., Diez, S., and Janson, M.E. (2011). Adaptive braking by Ase1 prevents overlapping microtubules from sliding completely apart. Nat Cell Biol *13*, 1259–1264.

Cahu, J., Olichon, A., Hentrich, C., Schek, H., Drinjakovic, J., Zhang, C., Doherty-Kirby, A., Lajoie, G., and Surrey, T. (2008). Phosphorylation by Cdk1 increases the binding of Eg5 to microtubules in vitro and in Xenopus egg extract spindles. PLoS ONE *3*, e3936.

Cai, S., Weaver, L.N., Ems-McClung, S.C., and Walczak, C.E. (2009). Kinesin-14 Family Proteins HSET/XCTK2 Control Spindle Length by Cross-Linking and Sliding Microtubules. Mol Biol Cell *20*, 1348–1359.

Chandra, R., Salmon, E.D., Erickson, H.P., Lockhart, A., and Endow, S.A. (1993). Structural and functional domains of the Drosophila ncd microtubule motor protein. J Biol Chem *268*, 9005–9013.

Fink, G., Hajdo, L., Skowronek, K.J., Reuther, C., Kasprzak, A.A., and Diez, S. (2009). The mitotic kinesin-14 Ncd drives directional microtubule-microtubule sliding. Nat Cell Biol *11*, 717–723.

Fu, C., Ward, J.J., Loïodice, I., Velve-Casquillas, G., Nedelec, F.J., and Tran, P.T. (2009). Phospho-regulated interaction between kinesin-6 Klp9p and microtubule bundler Ase1p promotes spindle elongation. Dev Cell *17*, 257–267.

Furuta, K., Furuta, A., Toyoshima, Y.Y., Amino, M., Oiwa, K., and Kojima, H. (2013). Measuring collective transport by defined numbers of processive and nonprocessive kinesin motors. Proc Natl Acad Sci USA *110*, 501–506.

Goshima, G., Nédélec, F., and Vale, R.D. (2005). Mechanisms for focusing mitotic spindle poles by minus end-directed motor proteins. J Cell Biol *171*, 229–240.

Hentrich, C., and Surrey, T. (2010). Microtubule organization by the antagonistic mitotic motors kinesin-5 and kinesin-14. J Cell Biol *189*, 465–480.

Hunt, A.J., Gittes, F., and Howard, J. (1994). The force exerted by a single kinesin molecule against a viscous load. Biophys J *67*, 766–781.

Hyman, A.A., Weber, C.A., and Jülicher, F. (2014). Liquid-liquid phase separation

in biology. Annu Rev Cell Dev Biol *30*, 39–58.

Janson, M.E., Loughlin, R., Loïodice, I., Fu, C., Brunner, D., Nedelec, F.J., and Tran, P.T. (2007). Crosslinkers and motors organize dynamic microtubules to form stable bipolar arrays in fission yeast. Cell *128*, 357–368.

Johann, D., Goswami, D., and Kruse, K. (2015). Generation of Stable Overlaps between Antiparallel Filaments. Phys Rev Lett *115*, 118103.

Kapitein, L.C., Peterman, E.J.G., Kwok, B.H., Kim, J.H., Kapoor, T.M., and Schmidt, C.F. (2005). The bipolar mitotic kinesin Eg5 moves on both microtubules that it crosslinks. Nature *435*, 114–118.

Karabay, A., and Walker, R. (1999). Identification of microtubule binding sites in the Ncd tail domain. Biochemistry *38*, 1838–1849.

Khmelinskii, A., Roostalu, J., Roque, H., Antony, C., and Schiebel, E. (2009). Phosphorylation-dependent protein interactions at the spindle midzone mediate cell cycle regulation of spindle elongation. Dev Cell *17*, 244–256.

Kusumi, A., Sako, Y., and Yamamoto, M. (1993). Confined lateral diffusion of membrane receptors as studied by single particle tracking (nanovid microscopy). Effects of calcium-induced differentiation in cultured epithelial cells. Biophys J *65*, 2021–2040.

Kwon, M., Godinho, S.A., Chandhok, N.S., Ganem, N.J., Azioune, A., Théry, M., and Pellman, D. (2008). Mechanisms to suppress multipolar divisions in cancer cells with extra centrosomes. Genes Dev *22*, 2189–2203.

Lansky, Z., Braun, M., Lüdecke, A., Schlierf, M., Wolde, ten, P.R., Janson, M.E., and Diez, S. (2015). Diffusible crosslinkers generate directed forces in microtubule networks. Cell *160*, 1159–1168.

Lecland, N., and Lüders, J. (2014). The dynamics of microtubule minus ends in the human mitotic spindle. Nat Cell Biol *16*, 770–778.

Lupas, A., Van Dyke, M., and Stock, J. (1991). Predicting coiled coils from protein sequences. Science *252*, 1162–1164.

Mana-Capelli, S., McLean, J.R., Chen, C.-T., Gould, K.L., and McCollum, D. (2012). The kinesin-14 Klp2 is negatively regulated by the SIN for proper spindle elongation and telophase nuclear positioning. Mol Biol Cell *23*, 4592–4600.

Patel, A., Lee, H.O., Jawerth, L., Maharana, S., Jahnel, M., Hein, M.Y., Stoynov, S., Mahamid, J., Saha, S., Franzmann, T.M., et al. (2015). A Liquid-to-Solid Phase Transition of the ALS Protein FUS Accelerated by Disease Mutation. Cell *162*, 1066–1077.

Ruhnow, F., Zwicker, D., and Diez, S. (2011). Tracking Single Particles and Elongated Filaments with Nanometer Precision. Biophys J *100*, 2820–2828.

Schuyler, S.C., Liu, J.Y., and Pellman, D. (2003). The molecular function of Ase1p: evidence for a MAP-dependent midzone-specific spindle matrix. Microtubule-associated proteins. J Cell Biol *160*, 517–528.

Sturgill, E.G., Das, D.K., Takizawa, Y., Shin, Y., Collier, S.E., Ohi, M.D., Hwang, W., Lang, M.J., and Ohi, R. (2014). Kinesin-12 Kif15 targets kinetochore fibers through an intrinsic two-step mechanism. Curr Biol *24*, 2307–2313.

Tao, L., Mogilner, A., Civelekoglu-Scholey, G., Wollman, R., Evans, J., Stahlberg, H., and Scholey, J.M. (2006). A Homotetrameric Kinesin-5, KLP61F, Bundles Microtubules and Antagonizes Ncd in Motility Assays. Curr Biol *16*, 2293–2302.

Watts, C.A., Richards, F.M., Bender, A., Bond, P.J., Korb, O., Kern, O., Riddick, M., Owen, P., Myers, R.M., Raff, J., et al. (2013). Design, synthesis, and biological evaluation of an allosteric inhibitor of HSET that targets cancer cells with supernumerary centrosomes. Chem Biol *20*, 1399–1410.

Yamashita, A. (2005). The Roles of Fission Yeast Ase1 in Mitotic Cell Division, Meiotic Nuclear Oscillation, and Cytokinesis Checkpoint Signaling. Mol Biol Cell *16*, 1378–1395.

Figures

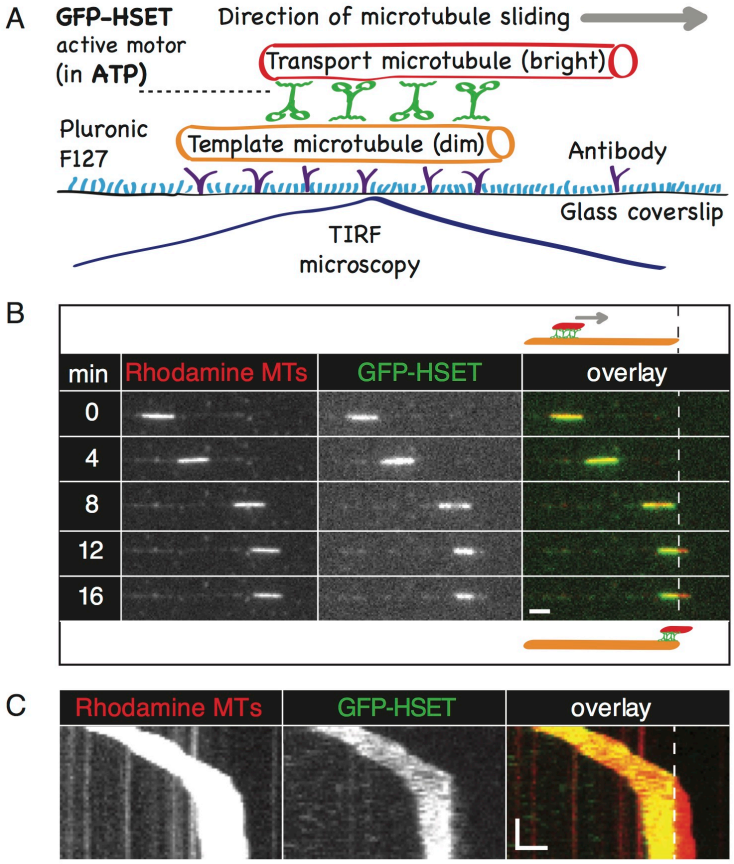

Figure 1. HSET propelled microtubule sliding slows down when microtubules start to separate. (**A**) Schematic representation of GFP-HSET-driven sliding of a transport microtubule along a surface-immobilized template microtubule. (**B**) Time-lapse fluorescence micrographs of the transport microtubule sliding along a template microtubule (red) at 1.5 nM GFP-HSET (green) concentration. Fully overlapping microtubules initially slide at a constant velocity. Sliding slows down when the microtubules start to separate. Dashed line indicates the position of the minus end of the template microtubule. The schematic diagrams indicates the positions of template (orange) and transport (red) microtubules in the beginning and at the end of the experiment, respectively. (**C**) Multichannel kymograph representing time-lapse fluorescence data presented in panel (B). The slope is initially constant, indicating a constant sliding velocity, until the transport microtubule reaches the end of the template microtubule, causing a drastic decrease in sliding velocity. Scale-bars are 2 μm horizontal and 5 min vertical. Grey arrows indicate the direction of microtubule sliding.

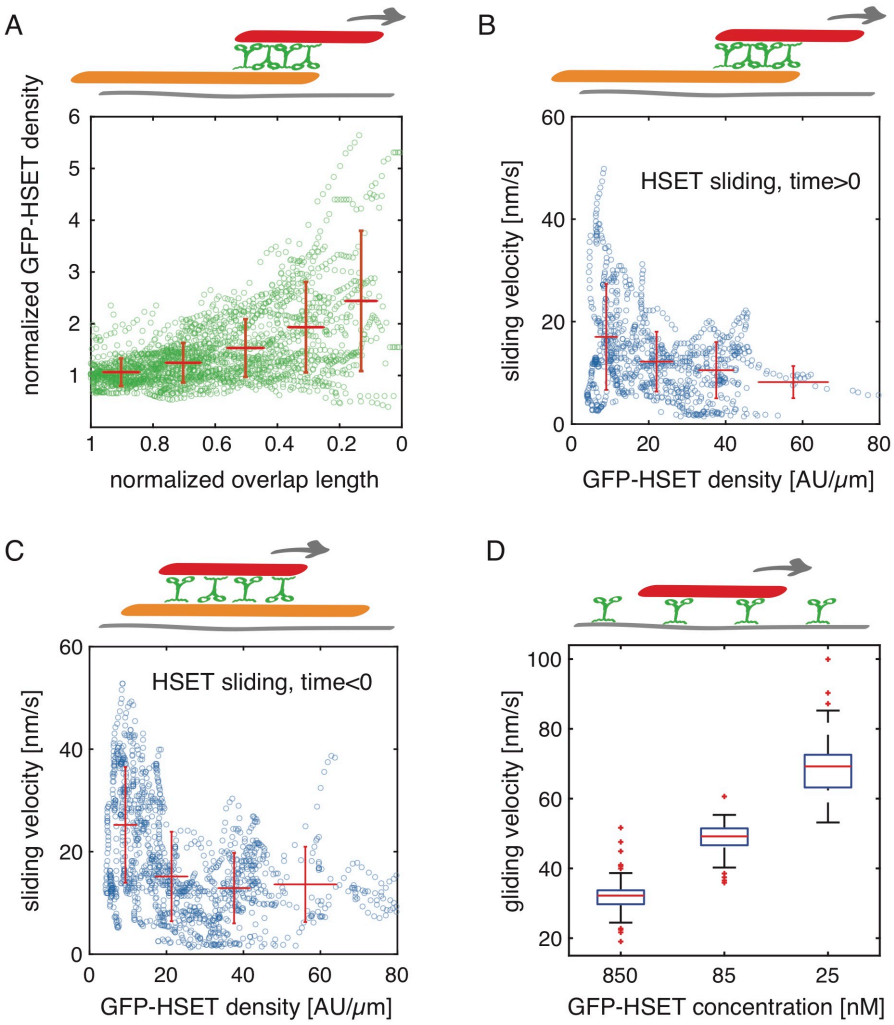

Figure 2. HSET-driven microtubule movement slows down with increasing density of motors. (**A**) The density of GFP-HSET (defined as the intensity of GFP-HSET fluorescence in AU per unit length) increases as the microtubule overlap shortens when two microtubules slide apart (during events such as presented in Figure 1). The GFP-HSET density and the overlap length were normalized to unity at the moment when the microtubules started to slide apart. Green data points indicate combined measurements of 33 microtubules sliding apart. Red crosses indicate binned and averaged values (± SD). (**B**) The increase in density of GFP-HSET in the microtubule overlaps when the microtubules slide apart (in panel A) correlates with a decrease in the velocity of microtubule sliding. Blue data points indicate combined measurements of 33 microtubules sliding apart. Red data crosses indicate binned and averaged values (± SD). (**C**) Higher density of GFP-HSET between fully overlapping microtubules correlates

with higher velocity of microtubule sliding. Blue data points indicate combined measurements of 67 sliding microtubules. Red data crosses indicate binned and averaged values (± SD). (**D**) The velocity of microtubule gliding, propelled by surface-immobilized HSET molecules, as a function concentration of HSET in solution used for the surface coating, which sets the density of the HSET motors on the coverslip surface. Gliding experiments were performed at three different HSET concentrations, namely 25 nM (n = 88), 85 nM (n = 75) and 850 nM (n = 82). For microtubules longer than approximately 1.5 μm, which were analyzed here, the velocity of gliding was independent of microtubule length (Figure S2A), suggesting that above a certain number of motors, the gliding velocity is independent of the motor number but dependent on their density. Schematic representations above the panels demonstrate the geometry of the experimental setup. Grey arrows indicate the direction of microtubule sliding.

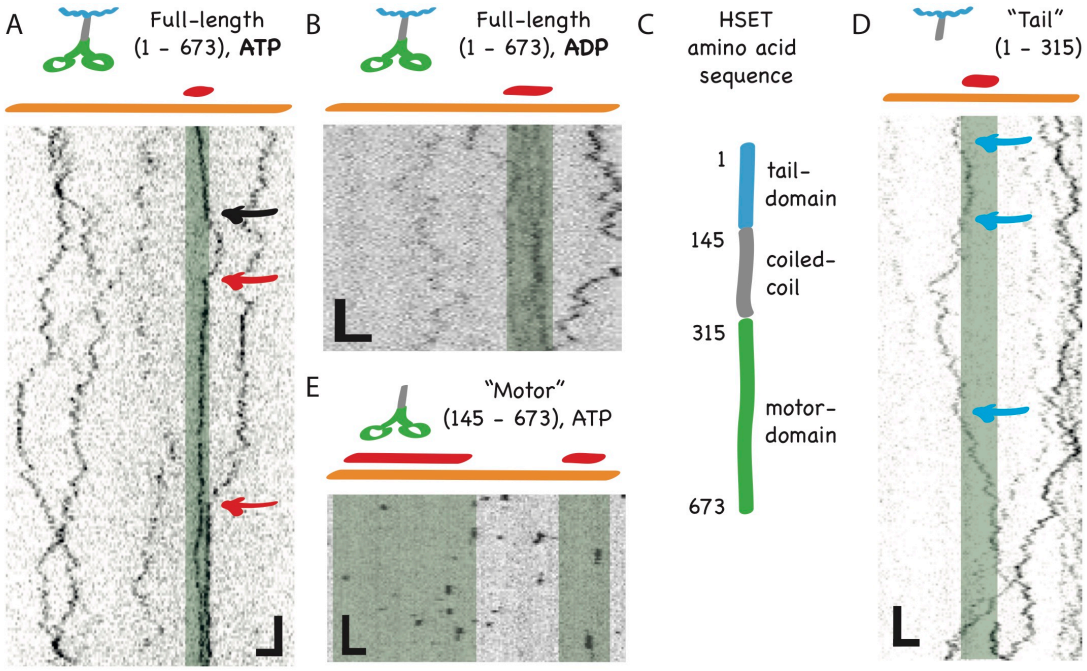

Figure 3. HSET diffuses fast on single microtubules and slowly in microtubule overlaps, with the overlap ends forming diffusion barriers. (**A**) Kymograph showing single GFP-HSET molecules at concentration of 0.1 nM diffusing along a single microtubule and in a microtubule overlap (in the presence of ATP). The position of the microtubule overlap is indicated by the grey transparent box overlaid with the kymograph. Occasionally, single GFP-HSET molecules were observed to enter (red arrow) or leave the overlap (black arrow). (**B**) Kymograph showing single GFP-HSET molecules at concentration of 0.15 nM diffusing along a single microtubule and in a microtubule overlap (in the presence of ADP and in the absence of ATP). Diffusion does not depend on the nucleotide state of HSET molecules - compare to panel (A). Microtubule overlaps are indicated as in (A). (**C**) Schematic representation of the HSET amino-acid sequence. (**D**) and (**E**) Kymographs showing the interaction of 0.1 nM GFP-HSET-tail (D) and 0.1 nM GFP-HSET-motor-domain (E) with single microtubules and microtubule overlaps. Microtubule overlaps were formed using 0.15 nM unlabeled HSET. In contrast to the full-length GFP-HSET, GFP-HSET-tail diffuses freely across the overlap ends (D; events marked by blue arrows). The GFP-HSET-motor-domain (E) interacts very shortly with both, single microtubules and with microtubule overlaps. Scale bars are 2 μm horizontal and 2 s vertical.

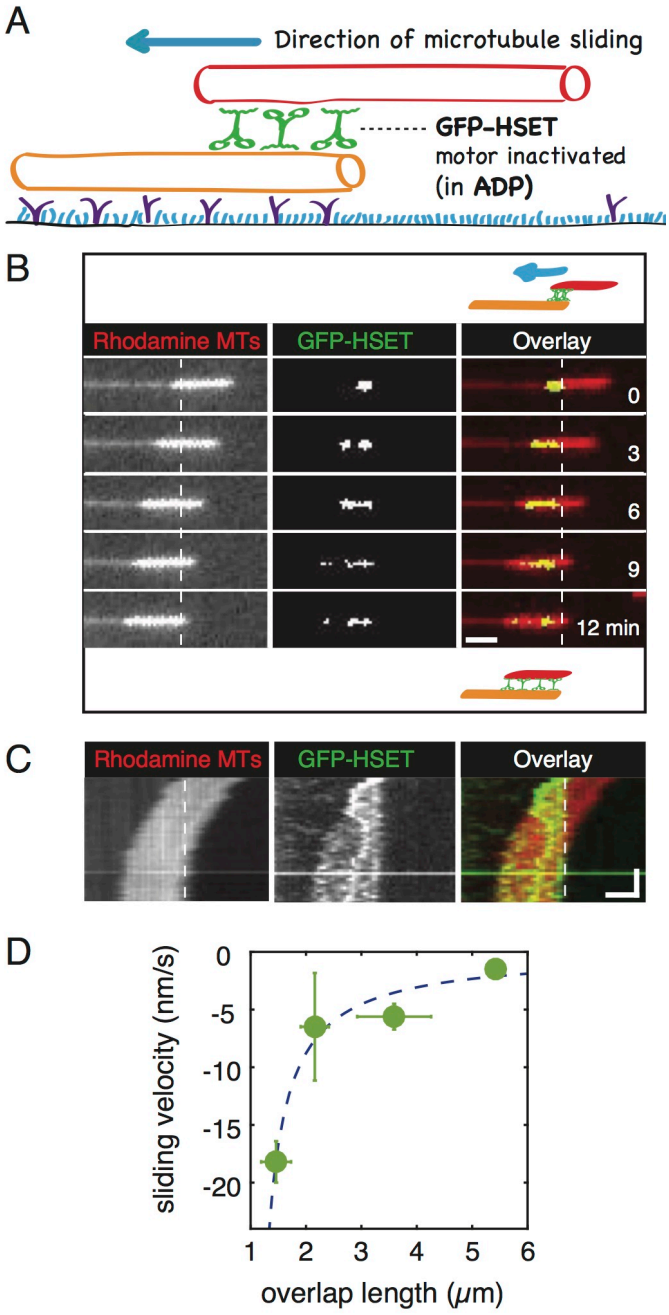

Figure 4. HSET generates entropic forces, which increase the size of the overlap region in the absence of ATP hydrolysis. (**A**) Schematic representation of the experiment with HSET sliding in the presence of ADP (in the absence of ATP). (**B**) Time-lapse fluorescence micrographs of the transport microtubule sliding along a template microtubule (red) driven by ADP-bound GFP-HSET (green) confined in the overlap region. All unbound GFP-HSET was removed from solution before the beginning of imaging. Transport microtubules always move in direction of increasing the overlap length. Dashed line indicates the position of the minus end of the template microtubule. The schematic

diagram indicates the position of template (orange) and transport (red) microtubules in the beginning and at the end of the experiment. (**C**) Multichannel kymograph representing time-lapse fluorescence data presented in panel (B). Scale-bars are 5 min vertical and 3 μm horizontal. (**D**) The absolute value of the velocity of the overlap expansion decreases hyperbolically with the length of the microtubule overlap (n = 8 microtubule pairs; the overlap expansion in presence of ADP is expressed using negative values because the microtubules move in opposite direction compared to experiments in the presence of ATP). The hyperbolic dependence is a signature of entropic forces generated by the diffusible crosslinker molecules confined in the overlap (Lansky et al., 2015).

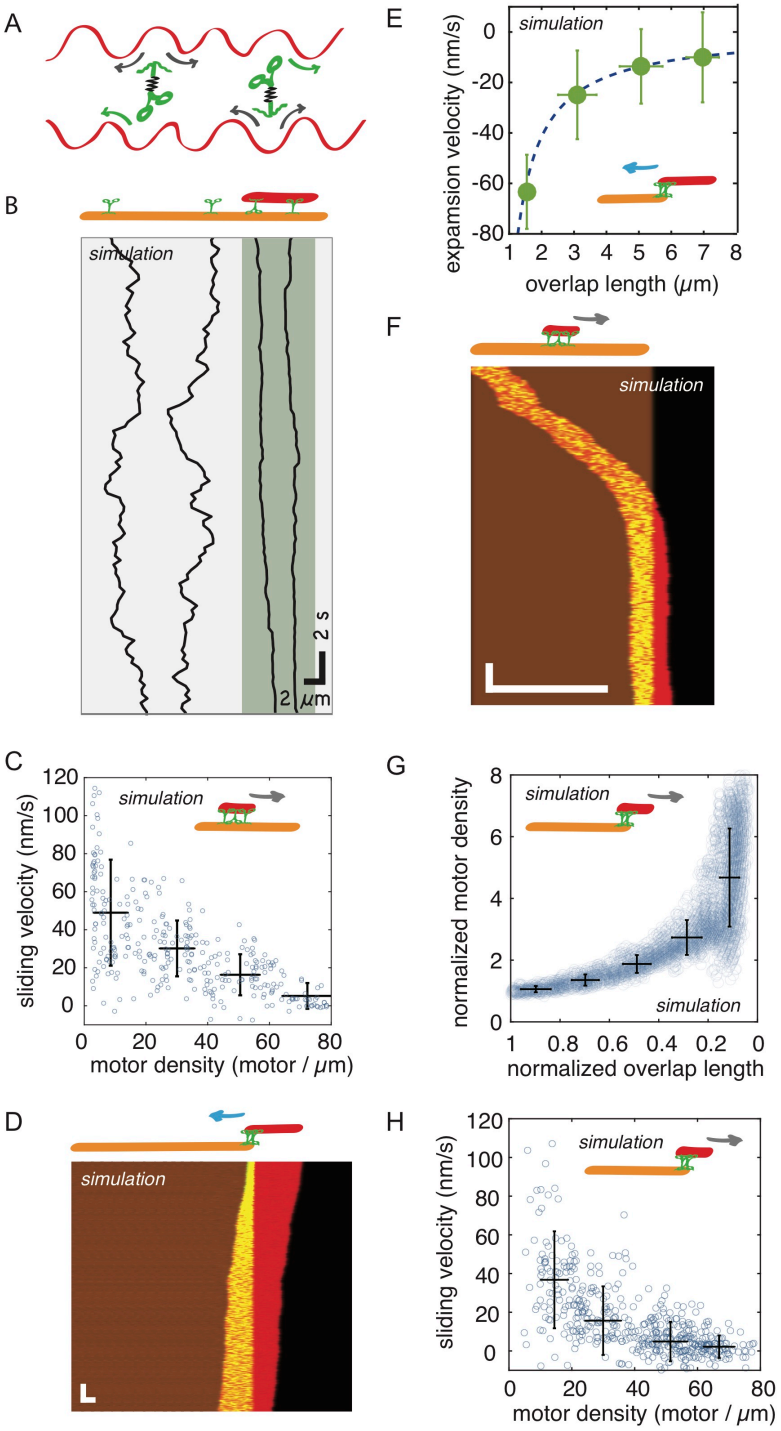

Figure 5. Simulation of diffusible molecular motors confined in the microtubule overlap explains the HSET autoregulatory mechanism. (**A**) Schematic representation of the modeled geometry. Microtubules are modeled as a one-dimensional array of binding sites. Molecular motors are simulated as harmonic springs, whose one end hops randomly (tail-domain) and the other end hops directionally (motor-domain) between neighboring binding sites on the microtubules (Methods). (**B**) Kymograph showing the simulated diffusion of

single molecular motor molecules along a single microtubule and in a microtubule overlap. The fast diffusion of the molecular motor on the single microtubule is mediated exclusively by the tail-domain. The slow diffusion of the molecular motor in the overlap is explained by the high binding and unbinding rate of its motor-domain (compare to experimental data in Figure 3A). The overlap is indicated by the darker grey area, cartoon on top of the kymograph represents the position of the template (orange) and transport (red) microtubules. Scale-bars are 2 μm horizontal and 2 s vertical. (**C**) Simulated velocity of sliding of fully overlapping microtubules decreases with increasing density of motors in the overlap (n = 22 simulated sliding microtubules; blue points indicate the simulated data, black crosses indicate the binned and averaged values (± SD); compare to experimental data in Figure 2C). (**D**) Simulated kymograph of microtubule sliding driven by molecular motors in the absence of ATP (in presence of ADP; compare to experimental data in Figure 4C). ATP-independent microtubule sliding was simulated using the molecular motors described in (B), which had their maximum force set to zero (Methods). 5 s vertical, 1 μm horizontal scale bars. (**E**) The absolute value of the simulated velocity of overlap expansion decreases hyperbolically with the length of the microtubule overlap in events as presented in (D) (n = 9 simulated microtubule pairs; ATP-independent velocity is expressed using negative values; compare to experimental data in Figure 4D). The hyperbolic dependence is a signature of an entropic origin of the forces generated by the diffusible crosslinker molecules confined in the overlap (Lansky et al., 2015). 5 s vertical, 1 μm horizontal scale bars. (**F**) Kymograph representation of a simulated event of molecular-motor driven sliding of a transport microtubule over the end of a template microtubule. In agreement with the experimental data, we observed that the transport microtubule slowed down as the two microtubules started sliding apart, resulting in the formation of a stable microtubule overlap (compare to Figure 1C). (**G**) The density of molecular motors in the overlap increases as the microtubules start to slide apart in events as presented in (F) (n = 15 simulated microtubule pairs; blue points indicate the simulated data, black crosses indicate the binned and averaged values (± SD)). Molecular motor density and the overlap length were normalized to unity at the moment when the microtubules

started to slide apart (compare to experimental data in Figure 2A). (**H**) Increasing density of molecular motors in the shortening microtubule overlaps in events as shown in (F) correlates with decreasing velocity of microtubule sliding (n = 15 simulated microtubule pairs; blue points indicate the simulated data, black crosses indicate the binned and averaged values (± SD); compare to experimental data in Figure 2B).

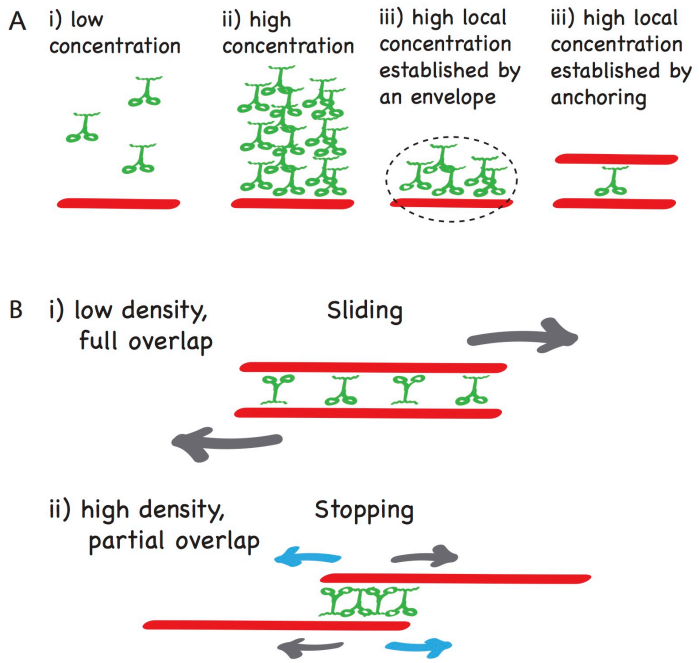

Figure 6. Simulation of diffusible molecular motors confined in the microtubule overlap explains the HSET autoregulatory mechanism. (**A**) The rate of binding of the motor-domain to its binding site on a microtubule is lower at (i) low concentration than at (ii) high concentration. Encapsulating the molecular motors in (iii) a membranous envelope or (iv) anchoring them by their tail-domains to an adjacent microtubule raises the effective local concentration adjacent to the microtubule and increases their net binding rate. (**B**) Schematic representation of the autoregulatory mechanism of HSET molecular motors: as microtubules start to slide apart, the diffusible HSET molecules are retained within the overlap region, leading to the HSET-density-dependent decrease in sliding velocity (grey arrows) and an entropic force resisting the sliding (blue arrows). This feedback mechanism results in the formation of stable microtubule overlaps.

Supplementary Material

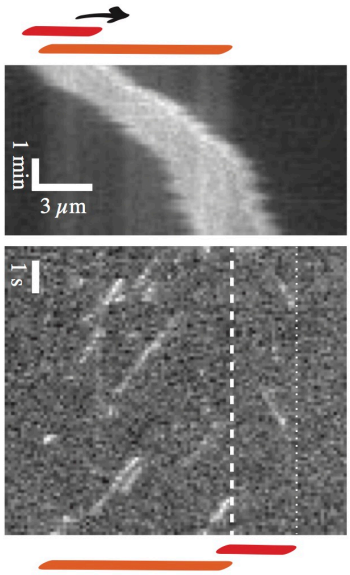

Figure S1. HSET slides antiparallel microtubules. Upper panel shows a kymograph representing HSET-propelled sliding of transport microtubule along a surface-immobilized template microtubule. Transport microtubule slowed down when sliding off the template and a stable microtubule overlap was established. Lower panel shows the movement of single GFP-labeled kinesin-1 molecules along the microtubules shown in the upper panel once the stable microtubule overlap was established. Vertical dashed line represents the end of the template microtubule; vertical dotted line represents the end of the transport microtubule. Movement of plus-end directed kinesin-1-GFP molecules indicates that the HSET-stabilized microtubule pair is in antiparallel orientation.

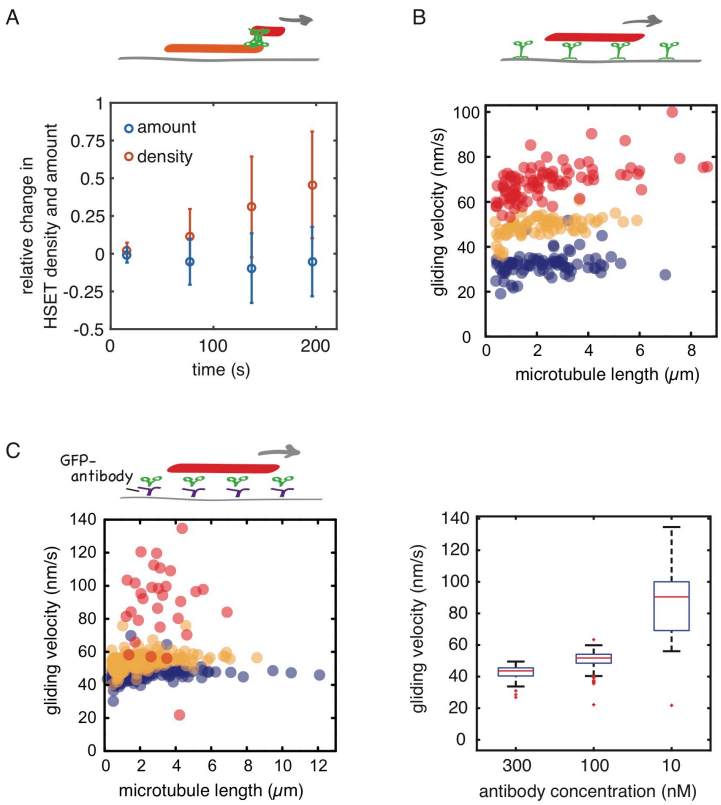

Figure S2. HSET driven microtubule movement slows down with increasing density of motors. (**A**) The amount of GFP-HSET molecules in the shortening overlaps remained constant as the microtubules slid apart (time t = 0 corresponds to the moment, when microtubules started to separate), leading to progressive increase in GFP-HSET densities in the shortening overlaps. The data represent binned and averaged values (± SD; n = 33). (**B**) Displacement-weighted velocities (Alper et al., 2013) of microtubule gliding propelled by HSET molecules, immobilized on a casein-coated surface, as a function of the length of the microtubule (same data as in Figure 2D). Gliding assays were performed at three different concentrations of HSET used for the coating of the surface: 25 nM (n = 88, red), 85 nM (n = 75, yellow) and 850 nM (n = 82, blue), which set different surface densities of the GFP-HSET molecules. Each data point represents a single gliding microtubule. At a given GFP-HSET concentration, the longer microtubules have more GFP-HSET molecules attached than the shorter ones. For microtubules longer than approximately 1.5 μm, the velocity of gliding was independent of microtubule length, suggesting that above certain number of motors, the gliding velocity is independent of the motor number but dependent on their density. (**C**) Left panel: The displacement–weighted velocity of

microtubule gliding, propelled by surface-immobilized molecules of the HSET-motor-domain construct, as a function of the length of the gliding microtubules. Gliding assays were performed at three different concentrations of HSET-motor-domain used for the coating of the coverslip surface: 10 nM (n = 124, red), 100 nM (n = 195, yellow), 300 nM (n = 30, blue), which set different surface densities of the motor-domains coating the coverslip surface. For microtubules longer than approximately 1.5 μm, which were analyzed here, the velocity of gliding was independent of microtubule length, suggesting that above certain number of motors, the gliding velocity is independent of the motor number but dependent on their density. Right panel: Median microtubule gliding velocities of the data shown in the left panel as a function of the HSET-motor-domain concentration represented in a box-and whisker plot.

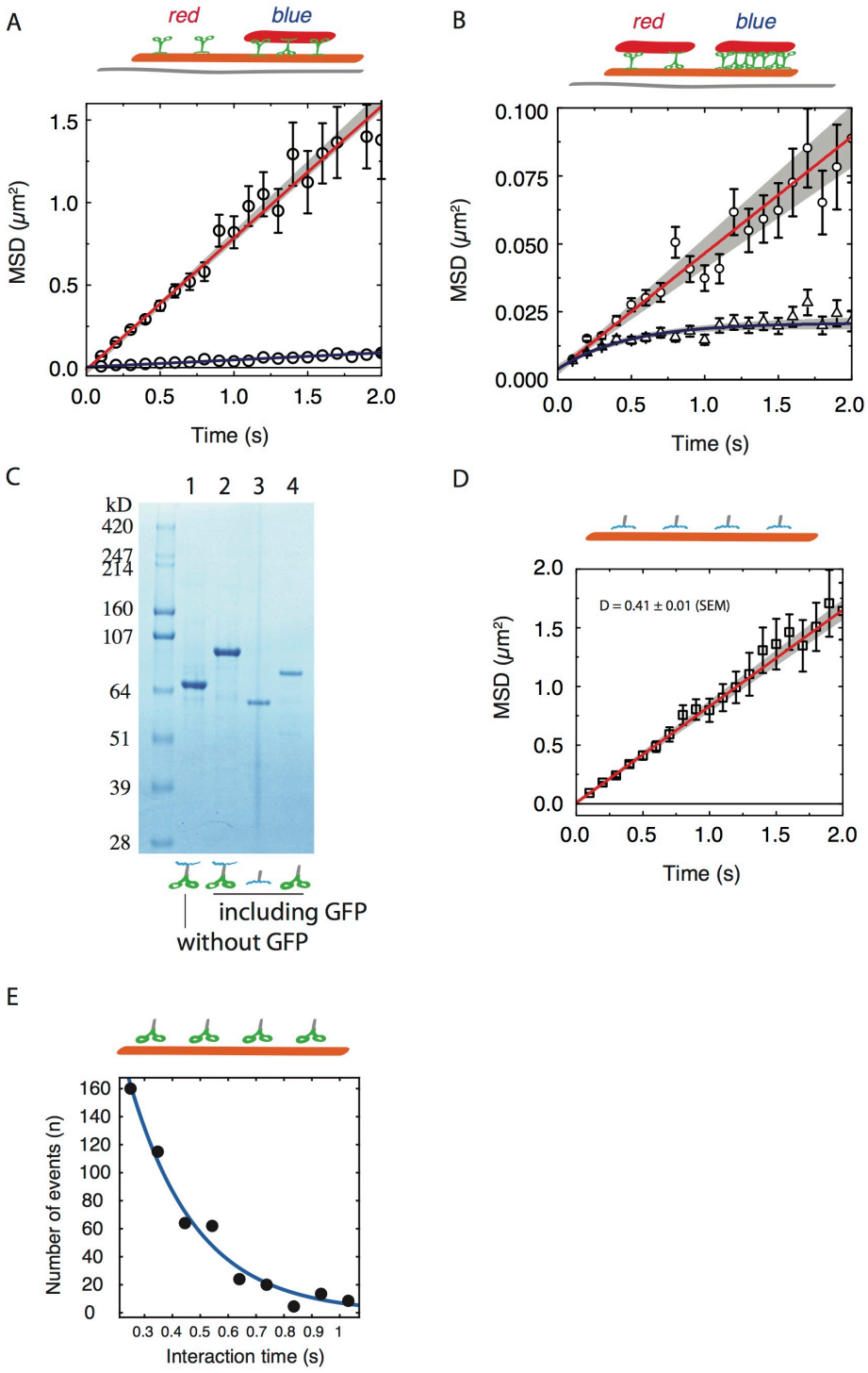

Figure S3. Interaction of the full-length and the truncated HSET constructs with microtubules. (**A**) Cumulative mean square displacement over time of diffusion events of the full length GFP-HSET on a single microtubule (N = 22) (red) and in the microtubule overlap (N = 14) (blue). A weighted linear fit to the data provides a diffusion constant of 0.39 ± 0.01 μm² s⁻¹ (± SEM) and 0.021 ± 0.005 μm² s⁻¹ (± SEM), respectively, gray 95% confidence band. (**B**)Mean square displacement analysis of single GFP-HSET molecules diffusing in the microtubule

overlap suggests that HSET molecules cannot pass each other: Cumulative mean square displacement over time of diffusion events of GFP-HSET in the microtubule overlaps for two different densities of HSET in the overlap. Circles (N = 14) represent data, where average distance between neighboring molecules (calculated as the length of the overlap divided by the average number of molecules in the overlap) was L > 500 nm. On 2 second timescale we observe free diffusion regime. A weighted linear fit (red) to the data provides a diffusion constant of D=0.021+-0.005 $\mu m^2/s$ (± SEM). Triangles (N = 22) represent data, where average distance L between neighboring molecules was between 250 and 430 nm. Blue line represents a weighted fit of the model of diffusion confined in boundaries (equation 11a from (Kusumi et al., 1993) to the data providing a diffusion constant of 0.026 ± 0.015 $\mu m^2/s$ (± SEM) and the distance between the boundaries L_B = 354 ± 25 nm $\mu m^2/s$ (95% confidence band - grey). The distance between the boundaries corresponds to the average distance between neighboring molecules suggesting that the molecules of HSET cannot pass each other in the microtubule overlap. (**C**) SDS-PAGE of the HSET constructs used in our experiments: [1] HSET (78 kd), [2] GFP-HSET (104 kD), [3] GFP-HSET-Tail (66 kD) and [4] GFP-HSET-Motor (90 kD). (**D**) Cumulative mean square displacement over time of diffusion events of GFP-HSET-tail on microtubules (N = 22). A weighted linear fit to the data (red) provides a diffusion constant of 0.41+-0.02 (± SEM), gray 95% confidence band. (**E**) Distribution of interaction times of the GFP-HSET-motor construct with microtubules as estimated from single molecule traces acquired in experiment presented in Figure 3C; single exponential fit provides the rate of unbinding of 4.1 ± 0.9 s^{-1} (95 % confidence interval).

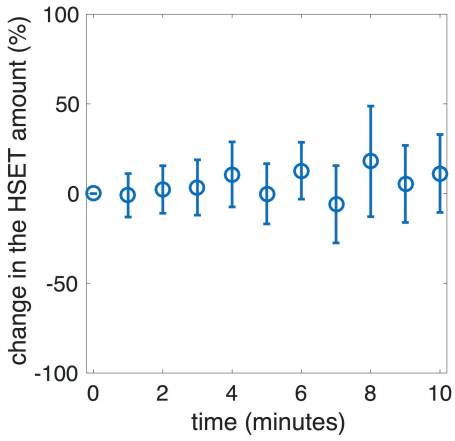

Figure S4. The amount of GFP HSET molecules in the overlap is constant during ATP-independent overlap expansion. The amount of GFP-HSET molecules in the microtubule overlap during sliding was estimated from the integrated GFP intensity in the overlap in experiments as presented in Figure 4. The data points represent binned and averaged values (± SD; n = 8 microtubule overlaps).

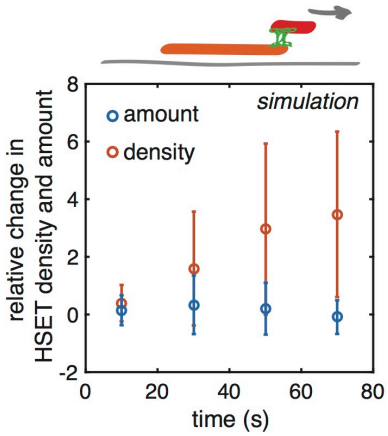

Figure S5. The amount of simulated HSET molecules stays constant during sliding apart, leading to the increase in HSET density in the shortening overlap. Time t = 0 corresponds to the moment, when microtubules started to separate.

Methods

Protein purification. Full length N-terminal hexa-histidine tagged HSET (1-673 aa) and GFP-HSET (1-673 aa) were expressed in Drosophila SF9 insect cells using Bac-to-Bac Expression System (Invitrogen). N-terminal hexa-histidine tagged GFP-HSET-tail (1-315 aa) and GFP-HSET-motor (145-673aa) were expressed in insect cells using flashBAC System (Oxford Expression Technologies). Harvested cells were resuspended in purification buffer (50 mM sodium phosphate buffer pH 7.5, 1 mM MgCl2, 10 mM 2-mercaptoethanol, 300 mM NaCl, 0.1% Tween20 w/vol, 10% glycerol w/vol, 30 mM imidazole and EDTA-free protease inhibitors (Roche)). Crude lysate was centrifuged at 20,000g at 4˚C and loaded on NiNTA resin (Qiagen). The resin was washed with purification buffer containing 60 mM imidazole. Proteins were eluted in purification buffer containing 300 mM imidazole, snap-frozen in liquid nitrogen and stored at -80˚C. Size and purity of all constructs was checked by SDS-PAGE gel (Fig. S3B).

In vitro motility assay and imaging. In microtubule sliding experiments, template microtubules, transport microtubules and flow cells were prepared as described previously (Fink et al., 2009). In the first step, biotinylated dimly paclitaxel-stabilized rhodamine-labeled template microtubules in BRB80 (80 mM Pipes/KOH pH 6.9, 1 mM $MgCl_2$, 1 mM EGTA), were immobilized in a flow chamber using biotin antibodies (Sigma B3640, 40 µg ml^{-1} in PBS). In the second step the buffer in the flow cell was exchanged for the assay buffer (20mM HEPES pH7.2, 1mM EGTA, 75mM KCl, 2 mM $MgCl_2$, 1 mM ATP (+Mg), 10mM dithiothreitol, 0.5mg/ml casein, 10 µM paclitaxel, 0.1% Tween, 10% w/v sucrose, 20mM d-glucose, 110 µg/ml glucose oxidase and 20 µg/ml catalase). Thirdly, one of the HSET constructs in assay buffer was flushed into the flow cell at final assay concentrations. Fourthly, brightly rhodamine labeled, non-biotinylated transport microtubules in assay buffer were flushed into the flow cell and were allowed to bind to the template microtubules via HSET. Finally, the chamber was rinsed with assay buffer containing the HSET construct at the final assay concentration. This last step removed unbound transport microtubules from solution. For experiments showing HSET-dependent overlap expansion, the

buffer flush in the final step did not contain any HSET molecules. All experiments were performed at 24˚C.

In microtubule gliding experiments with the HSET full-length construct, detergent-cleaned coverslips were used to make the flow cell. In the first step, casein buffer (20mM HEPES pH7.2, 1mM EGTA, 75mM KCl, 2 mM $MgCl_2$, 0.5mg/ml casein) was flushed into the flow cell. In the second step, the HSET molecules in assay buffer were flushed into the flow cell. Thirdly, brightly rhodamine labeled microtubules were flushed in and allowed to bind to the HSET molecules. Finally, the chamber was rinsed with assay buffer to remove the unbound microtubules.

In case of the microtubule gliding experiments with the GFP-HSET-motor-domain, Dichlorodimethylsilane-silanized coverslips were used to make the flow cell. In the first step, GFP-HSET-motor-domain constructs were immobilized in a flow chamber using anti-GFP monoclonal antibodies (mouse, MPI-CBG antibody facility). Secondly, brightly rhodamine-labeled microtubules were flushed in and finally the chamber was rinsed with assay buffer. Rhodamine-labeled microtubules were visualized with the acquisition rate of 1 frame per second in the TRITC channel

In microtubule sliding experiments rhodamine-labeled microtubules and GFP-labeled HSET constructs were visualized sequentially by switching between TRITC and GFP channels using a setup described previously (Braun et al., 2013) with the acquisition rate of 1 frame per 5 seconds for the TRITC channel and 1 frame per 25 seconds for the GFP channel. To visualize the interaction of single GFP labeled molecules with microtubules the GFP channel acquisition was 1 frame per 100 miliseconds.

Image analysis. The microtubule sliding experiments were analyzed by custom written Matlab (Mathworks) routine. The position of the transport microtubule relative to the template microtubule was measured in each frame. Sliding velocity was calculated from positional data of the transport microtubules using a rolling frame average over 9 frames. When the template and transport microtubules were fully overlapping the location of the overlap was identified as the location of the transport microtubule. When the microtubules were sliding

apart, the location of this shortening overlap was estimated from the position of the trailing (minus) end of the transport microtubule and the position of the minus end of the template microtubule. The location of the overlap was used in every frame to estimate the overlap length and as a mask to read out the total amount of overlap-bound GFP-HSET. GFP-HSET signal in regions directly adjacent to the mask was subtracted as the background signals. The fluorescent signal of a single GFP-HSET molecule was determined as described previously (Braun et al., 2011). The density of GFP-HSET in the overlap was estimated as a number of HSET molecules per unit of the overlap length. The single molecules diffusion traces were tracked using FIESTA software (Ruhnow et al., 2011) and the diffusion constants were calculated from mean square displacement values.

Optical trapping

For optical trapping experiments, biotinilated Alexa647-labeled microtubules attached to streptavidin-coated microspheres (Spherotech) and GFP-HSET were used. Forces were measured by C-Trap optical tweezers (Lumicks) used in a dual trap mode. Sensitivity and stiffness of the trap were determined using an in-build calibration feature that fits a Lorentzian function to the power spectrum of the thermal fluctuations of a trapped bead. All force measurements were performed at a trap stiffness of 0.2 pN/nm, and the time traces were recorded with 50 kHz sampling rate. The beads were pulled apart at a constant velocity of 0.5 μm/s. The time traces were further analyzed and converted into force-distance curves using an in-build software. During the force measurement, microtubules and GFP-HSET were visualized by confocal imaging using 488 nm and 647 nm excitation wavelengths (Lumicks).

Mathematical modeling

Microtubules were modeled as one-dimensional arrays of binding sites for the molecular motors. HSET molecules were modeled as springs with two distinct microtubule-binding sites, motor-domain and tail-domain, at the opposite ends of the spring. The HSET molecules mutually exclude each other and cannot pass each other when bound to the microtubule as suggested by experimental evidence (Figure S5A).

An HSET molecule can bind from solution to a single microtubule with one of its binding sites with the rates $k_{on}^{motor(solution)}$ and $k_{on}^{tail(solution)}$. When an HSET molecule is bound with one of its binding site to a single microtubule, it can dissociate from it into solution with rates $k_{off}^{motor(solution)}$ and $k_{off}^{tail(solution)}$. An HSET molecule, which is bound (anchored) to one of the microtubules by one of its binding sites, can associate with the second microtubule by its second binding site with rates $k_{on}^{motor(anchored)}$ and $k_{on}^{tail(anchored)}$. An HSET molecule, which is bound by both of its binding sites to two microtubules, can dissociate from one of the microtubules by one of its binding sites with rates $k_{off}^{motor(anchored)}$ and $k_{off}^{tail(anchored)}$. The rates of (un)binding of an anchored HSET molecule are dependent on the tension of the spring as described in (Lansky et al., 2015). When bound to the microtubule the tail-domain can hop with equal probability k_+ = k_-, to the two neighboring (vacant) binding sites and was modeled as described earlier (Lansky et al., 2015). For the other binding site - the motor-domain - the hopping probabilities, k_+ and k_-, are asymmetric. The net speed of a single molecular motor is then v = \delta (k_+ - k_-). The maximum stall force of the molecular motor F_max is characterized as k_+ / k_- = exp[- \beta F_max \delta].

The parameters used for the simulation are summarized in the Supplementary Table S1. We assumed that, in the absence of tension on the spring, the values of anchored tail- and motor-domain unbinding $k_{off}^{tail(anchored)}$ and $k_{off}^{motor(anchored)}$ will be equal to the values of their unbinding to solution $k_{off}^{tail(solution)}$ and $k_{off}^{motor(solution)}$, respectively. The experimentally determined dwell time of the tail-domain on a microtubule is orders of magnitude longer than the dwell time of the motor-domain, suggesting that the interaction of the molecular motor with the microtubule will be predominantly tail-mediated. The effective diffusion constant D_d of an HSET molecule bound between two microtubules thus depends on the tail- and the motor-domain hopping rates and the attachment and the detachments rates of the motor-domain of a tail-anchored molecular motor $k_{on}^{motor(anchored)}$ and $k_{on}^{motor(anchored)}$. We exploited the dependence on $k_{on}^{motor(anchored)}$ to match D_d with the value measured experimentally. Binding from solution was set such that the steady state density of an HSET molecule bound to a microtubule would correspond to GFP-HSET

densities observed in our experiments. The algorithm used to simulate the model is described in (Lansky et al., 2015).

Table S1.

tail diffusion	0.4 $\mu m^2/s$	measured
motor maximum force	0.1 pN	(Furuta et al., 2013) *
motor max speed	0.1 μm/s	(Furuta et al., 2013)
spring stiffness	$5x10^4$ $k_BT\mu m^{-2}$	(Lansky et al., 2015)**
$k_{on}^{motor(anchored)}$	60 s^{-1}	fit***
$k_{off}^{motor(solution)}$	4 s^{-1}	measured
$k_{off}^{tail(solution)}$	0.01 s^{-1}	measured
diffusion of MT in solution	0.01 $\mu m^2/s$	(Hunt et al., 1994)
lattice spacing	0.01 μm	tubulin dimer length

* For simulation of the experiment in the absence of ATP (in presence of ADP), the motor maximum force was set to zero.

** The spring stiffness was set to a value estimated earlier for a different microtubule crosslinker. Our results are qualitatively independent of the spring stiffness in the range between $\sim 10^2$ - 10^4 $k_BT\mu m^{-2}$. For spring stiffness higher than $\sim 10^5$ $k_BT\mu m^{-2}$ we do not observe any sliding.

*** The $k_{on}^{motor(anchored)}$ was chosen such that the diffusion constant of a single molecular motor bound between two filaments is as observed in the experiment.